

Broadband Green's Function with Low Wavenumber Extraction for Arbitrary Shaped Waveguide and Applications to Modeling of Vias in Finite Power/Ground Plane

Leung Tsang* and Shaowu Huang

Abstract—In this paper we developed the method of broadband Green's function with low wavenumber extraction (BBGFL) for arbitrary shaped waveguide. The case of Neumann boundary condition is treated. The BBGFL has the advantage that when using it to solve boundary value problems in a waveguide, the boundary conditions have been satisfied already. The broadband Green's function is expressed in modal expansion of modes that are frequency independent. To accelerate the convergence of the Green's function, a low wavenumber extraction is performed. The singularity of the Green's function is also extracted by such low wavenumber extraction. Numerical results show that BBGLF and direct MoM are in good agreement. We next illustrate the application of BBGFL for broadband simulations of vias in printed circuit boards (PCB) by combining with the method of Foldy-Lax multiple scattering equation. The results show that BBGFL are in good agreement with MoM and HFSS. It is also shown that BBGFL is many times faster than direct MoM and HFSS. The computational efficiency in broadband simulations makes this technique useful for fast computer-aided design (CAD).

1. INTRODUCTION

The effects of waveguide or cavity structures are critical for the electrical performance of electronic devices and components in signal integrity (SI), power integrity (PI), electromagnetic interference (EMI), and electromagnetic compatibility (EMC). Harmful electromagnetic signal noises or interferences are often generated and amplified at the resonant frequencies of the waveguide or cavity structures. The issues deteriorate when the electronic devices or computer systems operate at higher frequency or faster speed. In printed circuit boards (PCBs), two adjacent power/ground planes form a waveguide/cavity structure. The propagating modes satisfy the PMC (Neumann boundary conditions) at the edges of PCB power/ground plane structures. The power/ground plane structures are the key root causes in SI/PI and EMI/EMC problems. Vias are used for vertical interconnects for multilayer PCBs. At frequencies near the resonant frequencies, the propagating electromagnetic waves excite resonant modes, that result in strong edge radiations. These cause EMI/EMC problems. The switching noises induced by voltage regulator module (VRM) generate voltage fluctuations and lead to PI problems. The high frequency power noise can also couple into signal vias and cause SI/PI coupling issues. Therefore, the modeling of PCB cavity with vias is critical in practical designs and applications of high speed PCBs and packages. Fast and accurate modeling technique is desired for broadband simulations in electronic design and application. The finiteness of the parallel power/ground planes make them waveguide/cavity structures. The power/ground planes are also of arbitrary shape. Commercial tools such as HFSS provide solutions for the analysis of the via-cavity coupling problem. The tools require large CPU and memory and are not suited for broadband analysis. The physical problem is that of TM modes in a cavity with PMC boundary conditions on the side walls. Various methods have been used for waveguide

Received 26 July 2015, Accepted 21 August 2015, Scheduled 27 August 2015

* Corresponding author: Leung Tsang (tsangl@uw.edu).

The authors are with the Department of Electrical Engineering, University of Washington, Seattle, WA 98195, USA.

problem of arbitrary shape [1–14]. For example, analytical methods were developed for rectangular structures [3, 4]. Numerical methods such as transmission matrix method [5], finite differential time domain (FDTD) method [6], and finite differential method (FDM) [7] were used for arbitrarily shaped structures. The boundary integral resonant mode expansion (BI-RME) method [8] was used to calculate the modes of arbitrarily shaped waveguide.

Green's function method with MoM has played an important role in the modeling waveguide/cavity structures and printed circuit boards (PCBs) [9–14]. The standard MoM method as in References [10, 11] consists of using the free space Green's function to formulate the integral equation. The disadvantage of the use of the free space Green's function is that, one solves the boundary value problem of an arbitrary shaped waveguide for each frequency. For broadband simulations, the dense MoM matrix equation needs to be solved many times leading to low computational efficiency. In this paper, a novel technique, the broadband Green's function with low wavenumber extraction (BBGFL), is proposed for fast and accurate modeling of problems in arbitrarily shaped waveguide/cavity structures. The technique is also applied to the problem of high speed interconnects. Broadband Green's functions exist for rectangular waveguide and circular waveguide [15]. In this paper we develop the broadband Green's function for waveguide of arbitrary shape. Unlike the MoM method in [10, 11], the MoM in BBGFL is solved only once for low wavenumber extraction.

Using the BBGFL method, we compute the modes of the arbitrary shape waveguide with a reference Green's function. Then we use the modes to construct the broadband Green's function. In addition, a low wavenumber extraction is introduced to accelerate the convergence of the modal expansion of the broadband Green's function. The merits of the methodology of BBGFL in this paper are: (1) a fast technique for computing the broadband Green's functions is developed; (2) the convergence of the modal expansion is accelerated using low wavenumber extractions; (3) with the low wavenumber extraction, the singularity of the broadband Green's function is also extracted, (4) the MoM with free space Green's function is used only once for the low wavenumber, and (5) the BBGFL is combined with the method of Foldy-Lax multiple scattering equations [9–14, 16–21] for fast and accurate field simulations of vias in arbitrarily shaped PCB power/ground planes.

2. METHODOLOGY

2.1. Broadband Bounded Green's Function with Low Frequency Extractions

In this section we derive the equations for the BBGFL technique and illustrate it for the L-shape waveguide. The methodology applies to waveguide of arbitrary shape. In Figures 1(a), and 1(b), we show respectively the rectangular waveguide with domain Ω and the L shape waveguide with domain

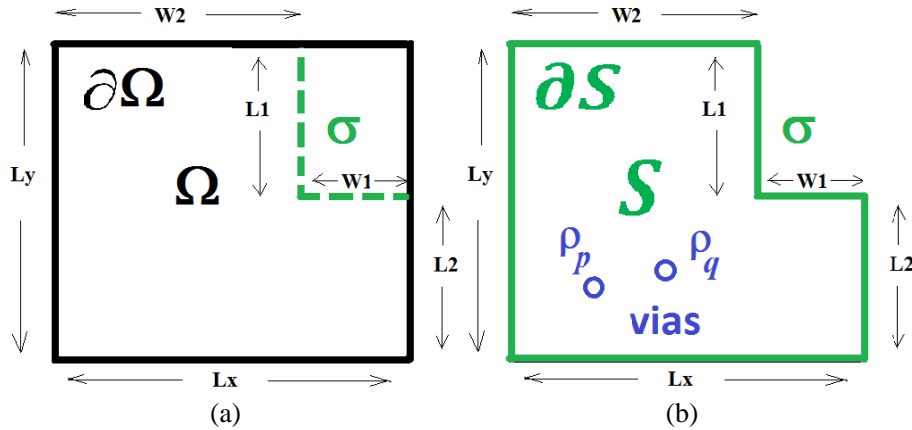


Figure 1. (a) Rectangle cavity Ω with boundary $\partial\Omega$. $g_H^\Omega(k, \bar{\rho}, \bar{\rho}')$ is Green's function with wavenumber k for Ω , $g_H^\Omega(k_L^\Omega, \bar{\rho}, \bar{\rho}') = g_0(k_L^\Omega, \bar{\rho}, \bar{\rho}') + g_{HR}^\Omega(k_L^\Omega, \bar{\rho}, \bar{\rho}')$ is Green's function at low wavenumber k_L^Ω . (b) L-shaped cavity S with boundary ∂S . $g_H^S(k, \bar{\rho}, \bar{\rho}')$ is Green's function with general wavenumber k for S , $g_H^S(k_L^S, \bar{\rho}, \bar{\rho}') = g_0(k_L^S, \bar{\rho}, \bar{\rho}') + g_{HR}^S(k_L^S, \bar{\rho}, \bar{\rho}')$ is Green's function at low wavenumber k_L^S .

S . The boundaries are $\partial\Omega$ and ∂S respectively. The boundary σ in Figures 1(a) and 1(b) is the part of ∂S that is not in $\partial\Omega$.

The problem in PCB consists of multiple vias in the L-shaped waveguide S . The BBGFL can be applied to many vias. For the sake of illustration of the technique, we showed two vias one centered at $\bar{\rho}_p$ and the other centered at $\bar{\rho}_q$ in Figure 1(b). The goal is to solve the problem in Figure 1(b) for a broad range of frequencies. The Green's function $g_H^\Omega(k, \bar{\rho}, \bar{\rho}')$ for rectangular waveguide Ω has been used in the BI-RME method [8]. The Green's function is at the wavenumber k . In this paper, we go beyond the rectangular waveguide Ω to develop the Green's function $g_H^S(k, \bar{\rho}, \bar{\rho}')$ for the L-shape waveguide S . The subscript H is to denote the Neumann boundary condition on the boundary $\partial\Omega$ and ∂S .

The physical problem in Figure 1(b) is that of TM modes with PMC on the boundary ∂S and PEC on the boundary of the vias. In waveguide problems with PEC side walls, the Neumann boundary condition corresponds to the TE case. However, in this present problem, it corresponds to the TM case. For the present problem, the wave function ψ represents the E_z component of the TM wave.

2.1.1. Broadband Green's Function $g_H^\Omega(k, \bar{\rho}, \bar{\rho}')$ and $g_H^S(k, \bar{\rho}, \bar{\rho}')$ with Low Wavenumber Extraction

Consider a rectangular waveguide Ω of dimensions L_x and L_y , $-\frac{L_x}{2} < x < \frac{L_x}{2}$, $-\frac{L_y}{2} < y < \frac{L_y}{2}$. The modal solutions are

$$\Psi_{mn}^\Omega(\bar{r}) = \sqrt{\frac{\xi_m \xi_n}{L_x L_y}} \cos \frac{m\pi}{L_x} \left(x + \frac{L_x}{2} \right) \cos \frac{n\pi}{L_y} \left(y + \frac{L_y}{2} \right) \quad (1)$$

where $m, n = 0, 1, 2, \dots$; $\xi_m = 2$ if $m \neq 0$; and $\xi_m = 1$ if $m = 0$. Let $k_{mn} = \sqrt{(k_{xm})^2 + (k_{yn})^2}$ be the resonant wavenumber of the rectangular waveguide Ω with $k_{xm} = \frac{m\pi}{L_x}$, $k_{yn} = \frac{n\pi}{L_y}$.

We use α as the combined index of (m, n) . Then

$$g_H^\Omega(k, \bar{\rho}, \bar{\rho}') = \sum_\alpha \frac{\psi_\alpha^\Omega(\bar{\rho}) \psi_\alpha^\Omega(\bar{\rho}')}{k_\alpha^2 - k^2} \quad (2)$$

In the BIRME method [8], the convergence of the modal expansion for the rectangular waveguide is accelerated by the extraction at DC. In the following, we use a low wavenumber extraction to accelerate the convergence. Note that the low wavenumber extraction is applicable for Ω as well as for the arbitrary waveguide S . Let the low wavenumber be k_L^Ω , which is much lower than the wavenumber of interest. That is $k_L^\Omega \ll k = \omega \sqrt{\mu\epsilon}$.

We calculate $g_H^\Omega(k_L^\Omega, \bar{\rho}, \bar{\rho}')$ as the sum of the free space Green's function and the response

$$g_H^\Omega(k_L^\Omega, \bar{\rho}, \bar{\rho}') = g_0(k_L^\Omega, \bar{\rho}, \bar{\rho}') + g_{HR}^\Omega(k_L^\Omega, \bar{\rho}, \bar{\rho}') \quad (3)$$

where

$$g_0(k_L^\Omega, \bar{\rho}, \bar{\rho}') = \frac{1}{4j} H_0^{(2)}(k_L^\Omega, \bar{\rho}, \bar{\rho}') \quad (4)$$

In Equations (3) and (4), $H_0^{(2)}$ is the 0th order Hankel function of the second kind, and $g_{HR}^\Omega(k_L^\Omega, \bar{\rho}, \bar{\rho}')$ is the response at the single low wavenumber k_L^Ω . In the appendix, we describe the calculations of the impedance matrix elements associated with the free space Green's function and the response Green's function for the low wavenumber k_L^Ω . Then the decomposition of $g_H^\Omega(k, \bar{\rho}, \bar{\rho}')$ is as follows

$$g_H^\Omega(k, \bar{\rho}, \bar{\rho}') = g_0(k_L^\Omega, \bar{\rho}, \bar{\rho}') + g_{HR}^\Omega(k_L^\Omega, \bar{\rho}, \bar{\rho}') + \sum_\alpha \frac{k^2 - (k_L^\Omega)^2}{(k_\alpha^2 - k^2) \left(k_\alpha^2 - (k_L^\Omega)^2 \right)} \psi_\alpha^\Omega(\bar{\rho}) \psi_\alpha^\Omega(\bar{\rho}') \quad (5)$$

Note that the modal expansion now converges as $1/k_\alpha^4$. Also $g_H^\Omega(k, \bar{\rho}, \bar{\rho}')$ needs only be calculated for $\bar{\rho}$ and $\bar{\rho}'$ on the L part of the boundary which is denoted as σ in Figure 1(b).

2.1.2. Calculation of $g_H^S(k, \bar{\rho}, \bar{\rho}')$ Modal Solution ψ_β^S and Resonant Wavenumber k_β^S

The Green's function for the L-shaped waveguide S is

$$g_H^S(k, \bar{\rho}, \bar{\rho}') = \sum_\beta \frac{\psi_\beta^S(\bar{\rho}) \psi_\beta^S(\bar{\rho}')}{(k_\beta^S)^2 - k^2} \quad (6)$$

where $\psi_\beta^S(\bar{\rho})$ is the modal solution of S and k_β^S the corresponding resonant wavenumber. Following a procedure similar to BI-RME [8], an integral equation approach is formulated to calculate $\psi_\beta^S(\bar{\rho})$ by using the $g_H^\Omega(k, \bar{\rho}, \bar{\rho}')$ with low wavenumber extraction and equivalent sources on σ . There are some differences from BI-RME in the matrix equation because we use low wavenumber extraction instead of DC extraction. The wave function ψ_H^S obeys the wave equation

$$(\nabla_t^2 + k^2) \psi_H^S = 0 \quad (7)$$

with Neumann boundary condition $\hat{n}_t \cdot \psi_H^S = 0$ on ∂S . Applying the Green's theorem to domain S to the two functions ψ_H^S , and g_H^Ω , there is a contribution from the surface integral on σ because g_H^Ω does not obey boundary condition on σ . The result integral equation is

$$-\psi_H^S(\bar{\rho}) = \int_\sigma dl' (\psi_H^S(\bar{\rho}') \hat{n}_t' \cdot \nabla_t' g_H^\Omega(k, \bar{\rho}, \bar{\rho}')) \quad (8)$$

Substitute $g_H^\Omega(k, \bar{\rho}, \bar{\rho}')$ from (5) into (8), we obtain

$$\psi_H^S(\bar{\rho}) = - \int_\sigma dl' \psi_H^S(\bar{\rho}') \hat{n}_t' \cdot \nabla_t' g_0(k_L^\Omega, \bar{\rho}, \bar{\rho}') - \int_\sigma dl' \psi_H^S(\bar{\rho}') \hat{n}_t' \cdot \nabla_t' g_{HR}^\Omega(k_L^\Omega, \bar{\rho}, \bar{\rho}') - \sum_\alpha b_\alpha \frac{\psi_\alpha(\bar{\rho})}{k_\alpha^2 - (k_L^\Omega)^2} \quad (9)$$

with

$$b_\alpha = \frac{k^2 - (k_L^\Omega)^2}{k_\alpha^2 - k^2} \int_\sigma dl' \psi_H^S(\bar{\rho}') \hat{n}_t' \cdot \nabla_t' \psi_\alpha(\bar{\rho}') \quad (10)$$

Equation (9) can be solved by the method of moments with point matching and pulse basis functions. Note that the singularity is only in the term containing the free space Green's function $\hat{n}_t' \cdot \nabla_t' g_0(k_L^\Omega, \bar{\rho}, \bar{\rho}')$ at low wavenumber k_L^Ω . We discretizing σ into N patches of Δt length each. Let the unknowns be

$$\psi_{Hn}^S = \frac{q_n}{\Delta t} \quad (11)$$

on σ_n , where σ_n is the n th patch on σ with $n = 1, 2, \dots, N$. Let the truncation of the modal expansion be at M terms, such that $\alpha = 1, 2, \dots, M$.

We define the matrix elements P_{mn} which is at a single low wavenumber k_L^Ω

$$P_{mn} = \left(\frac{1}{2}\right) \frac{1}{\Delta t} + \frac{1}{\Delta t} \int_{\sigma_m} dl' \hat{n}_t' \cdot \nabla_t' g_{HR}^\Omega(k_L^\Omega, \bar{\rho}_m, \bar{\rho}') \quad (12a)$$

for $n = m$, and

$$P_{mn} = \frac{1}{\Delta t} \int_{\sigma_n} dl' \hat{n}_t' \cdot \nabla_t' g_H^\Omega(k_L^\Omega, \bar{\rho}_m, \bar{\rho}') \quad (12b)$$

for $n \neq m$. Let

$$S_{m\alpha} = \left(\frac{1}{k_\alpha^2 - (k_L^\Omega)^2}\right) \psi_\alpha(\bar{\rho}_m) \quad (13)$$

In the appendix, we describe the method that we used to calculate P_{mn} .

In matrix notations

$$\bar{\bar{S}} \bar{b} + \bar{\bar{P}} \bar{q} = 0 \quad (14)$$

where $\bar{\bar{S}}$ is of dimension $N \times M$ with matrix elements described in (13), $\bar{\bar{P}}$ is of dimension $N \times N$ with matrix elements described in (12), \bar{b} is the unknown eigenvector of dimension $M \times 1$, and \bar{q} is of dimension $N \times 1$ with elements defined in (11).

Let

$$Q_{\alpha n} = \left(\frac{1}{k_{\alpha}^2 - (k_L^{\Omega})^2} \right) [\hat{n}'_t \cdot \nabla'_t \psi_{\alpha}(\bar{\rho}')]_{\bar{\rho}' = \bar{\rho}_n} \quad (15)$$

Then

$$b_{\alpha} = \frac{k^2 - (k_L^{\Omega})^2}{k_{\alpha}^2 - k^2} \left(k_{\alpha}^2 - (k_L^{\Omega})^2 \right) \sum_{n=1}^N Q_{\alpha n} q_n \quad (16)$$

Let

$$D_{\alpha\beta} = \left(\frac{1}{k_{\alpha}^2 - (k_L^{\Omega})^2} \right) \delta_{\alpha\beta} \quad (17)$$

Then, in matrix notations

$$\bar{\bar{D}} \bar{b} + \bar{\bar{Q}} \bar{q} = \frac{1}{k^2 - (k_L^{\Omega})^2} \bar{b} \quad (18)$$

where $\bar{\bar{D}}$ is of dimension $M \times M$ and $\bar{\bar{Q}}$ is of dimension $M \times N$.

Combining the two matrix Equations (14) and (17) gives the eigenvalue problem

$$\left(\bar{\bar{D}} - \bar{\bar{Q}} \bar{\bar{P}}^{-1} \bar{\bar{S}} \right) \bar{b} = \frac{1}{\tilde{k}^2} \bar{b} \quad (19)$$

with $\tilde{k}^2 = k^2 - (k_L^{\Omega})^2$. Solving the eigenvalue problem gives the resonant wavenumber k and the associated eigenvector \bar{b} . Note that $\bar{\bar{D}} - \bar{\bar{Q}} \bar{\bar{P}}^{-1} \bar{\bar{S}}$ is independent of k .

2.1.3. Normalization of Modes for Neumann Case

The size of the matrix eigenvalue equation in (19) is M . Let β be the eigenvalue index, k_{β}^S be the resonant wavenumber and $b_{\alpha\beta}$ be the eigenvector. After solving (19), we next normalize the modes $\psi_{\beta}^S(\bar{\rho})$.

Let

$$\tilde{\psi}_{\beta}^s(\bar{\rho}) = \sum_{\alpha=1}^M b_{\alpha\beta} \frac{\psi_{\alpha}(\bar{\rho})}{k_{\alpha}^2 - (k_L^{\Omega})^2} \quad (20)$$

Substitute (20) into (9) and apply ∇^2 . Then

$$\nabla^2 \tilde{\psi}_{\beta}^s(\bar{\rho}) = -\nabla^2 \psi_H^s(\bar{\rho}) + (k_L^{\Omega})^2 \int_{\sigma} dl' \psi_H^s(\bar{\rho}') \hat{n}'_t \cdot \nabla'_t g_H^{\Omega}(k_L^{\Omega}, \bar{\rho}, \bar{\rho}') \quad (21)$$

We discretize the L-shaped boundary σ , and use the discretized unknowns q_n . Equation (20) gives

$$(k_{\beta}^S)^2 \psi_{\beta}^s(\bar{\rho}) = \sum_{\alpha=1}^M b_{\alpha\beta} \frac{k_{\alpha}^2 \psi_{\alpha}(\bar{\rho})}{k_{\alpha}^2 - (k_L^{\Omega})^2} + (k_L^{\Omega})^2 \sum_{n=1}^N q_n [\hat{n}'_t \cdot \nabla'_t g_H^{\Omega}(k_L^{\Omega}, \bar{\rho}, \bar{\rho}')]_{\bar{\rho}' = \bar{\rho}_n} \quad (22)$$

2.1.3.1 Case of $k_{\beta} \neq 0$

Let the n th element of the column vector $\bar{\zeta}(\bar{\rho})$ be

$$[\bar{\zeta}(\bar{\rho})]_n = [\hat{n}'_t \cdot \nabla'_t g_H^{\Omega}(k_L^{\Omega}, \bar{\rho}, \bar{\rho}')]_{\bar{\rho}' = \bar{\rho}_n} \quad (23)$$

Then

$$(k_{\beta}^S)^2 \psi_{\beta}^s(\bar{\rho}) = \sum_{\alpha=1}^M b_{\alpha\beta} \frac{k_{\alpha}^2 \psi_{\alpha}(\bar{\rho})}{k_{\alpha}^2 - (k_L^{\Omega})^2} + (k_L^{\Omega})^2 [\bar{\zeta}^t(\bar{\rho})] \bar{q} \quad (24)$$

where t denotes the transpose of the matrix.

The normalization is

$$\iint_S dx dy (\psi_{\beta}^s(\bar{\rho}))^2 = \frac{1}{(k_{\beta}^S)^4} \iint_S dx dy \sum_{\alpha} \sum_{\alpha'} \left[\frac{b_{\alpha\beta} k_{\alpha}^2 \psi_{\alpha}(\bar{\rho})}{k_{\alpha}^2 - (k_L^{\Omega})^2} \frac{b_{\alpha'\beta} k_{\alpha'}^2 \psi_{\alpha'}(\bar{\rho})}{k_{\alpha'}^2 - (k_L^{\Omega})^2} \right]$$

$$\begin{aligned}
& + \frac{1}{(k_\beta^S)^2} \iint_S dxdy \sum_{\alpha'} \left[\frac{b_{\alpha'\beta} k_{\alpha'}^2 \psi_{\alpha'}(\bar{\rho})}{k_{\alpha'}^2 - (k_L^\Omega)^2} \right] \frac{(k_L^\Omega)^2}{(k_\beta^S)^2} [\bar{\zeta}^t(\bar{\rho})] \bar{q} \\
& + \frac{1}{(k_\beta^S)^2} \iint_S dxdy \sum_{\alpha} \left[\frac{b_{\alpha\beta} k_\alpha^2 \psi_\alpha(\bar{\rho})}{k_\alpha^2 - (k_L^\Omega)^2} \right] \frac{(k_L^\Omega)^2}{(k_\beta^S)^2} [\bar{\zeta}^t(\bar{\rho})] \bar{q} \\
& + \iint_S dxdy \left[\frac{(k_L^\Omega)^2}{(k_\beta^S)^2} [\bar{\zeta}^t(\bar{\rho})] \bar{q} \right]^2
\end{aligned} \tag{25}$$

We use the property $k_\alpha^2 \iint_S dxdy \psi_\alpha(\bar{\rho}) = 0$. Then

$$\iint_S dxdy (\psi_\beta^s(\bar{\rho}))^2 = \frac{1}{(k_\beta^S)^4} \sum_{\alpha} (b_{\alpha\beta})^2 \left(\frac{k_\alpha^2}{k_\alpha^2 - (k_L^\Omega)^2} \right)^2 + \iint_S dxdy \left[\frac{(k_L^\Omega)^2}{(k_\beta^S)^2} [\bar{\zeta}^t(\bar{\rho})] \bar{q} \right]^2 \tag{26}$$

Since $\iint_S dxdy (\psi_\beta^s(\bar{\rho}))^2 = 1$ and $k_L^\Omega \ll k_\beta^S$, the normalization condition for the eigenvector is

$$\sum_{\alpha=1}^M (b_{\alpha\beta})^2 = (k_\beta^S)^4 \tag{27}$$

2.1.3.2 Case of $k_\beta^S = 0$

The constant mode is a solution for the arbitrary waveguide with Neumann boundary condition. The constant mode for the L-shaped waveguide is

$$\psi_0^S(\bar{\rho}) = \sqrt{\frac{1}{A_S}} \tag{28}$$

where A_S = area of L-shaped waveguide.

2.1.4. Broadband Green's Function for L-shaped Waveguide and Low Wavenumber Extraction

After the normalized modal functions are calculated, the Green's function for the Neumann problem of the L-shaped waveguide is as given in Equation (6). The modal functions and eigenvalues are calculated by (19) for $k_\beta^S \neq 0$ and by (28) for $k_\beta^S = 0$. We will further use low wavenumber extraction for g_H^S of the arbitrary waveguide. Note that we use low wavenumber extraction, twice, with k_L^Ω for the rectangular waveguide and k_L^S for the waveguide with arbitrary shape. Let the solution be denoted by $g_H^S(k_L^S, \bar{\rho}, \bar{\rho}')$. When calculating the solution by MoM at k_L^S , the solution is separated into the sum of the primary $g_0(k_L^S, \bar{\rho}, \bar{\rho}')$ and the response $g_{HR}^S(k_L^S, \bar{\rho}, \bar{\rho}')$.

$$g_H^S(k_L^S, \bar{\rho}, \bar{\rho}') = g_0(k_L^S, \bar{\rho}, \bar{\rho}') + g_{HR}^S(k_L^S, \bar{\rho}, \bar{\rho}') \tag{29}$$

With the low wavenumber extraction the Green's function $g_H^S(k, \bar{\rho}, \bar{\rho}')$ for arbitrary k is

$$g_H^S(k, \bar{\rho}, \bar{\rho}') = g_0(k_L^S, \bar{\rho}, \bar{\rho}') + g_{HR}^S(k_L^S, \bar{\rho}, \bar{\rho}') + \sum_{\beta} \frac{k^2 - (k_L^S)^2}{\left((k_\beta^S)^2 - k^2 \right) \left((k_\beta^S)^2 - (k_L^S)^2 \right)} \psi_\beta^S(\bar{\rho}) \psi_\beta^S(\bar{\rho}') \tag{30}$$

Equation (30) is the result of the Broadband Green's function with low wavenumber extraction (BBGFL). Note that:

- i) The modal summation in (30) has convergence of $(k_\beta^S)^{-4}$;
- ii) The singularity of the Green's function in (30) has been subtracted and resides in the primary Green's function of the single low wavenumber, $g_0(k_L^S, \bar{\rho}, \bar{\rho}')$;

- iii) The wave functions $\psi_\beta^S(\bar{\rho})$, and resonant wavenumber k_β^S only depend on geometry. They are computed once and used for all frequencies;
- iv) The part of the expression that depends on frequencies and material properties are in k^2 in (30);
- v) The computations of broadband Green's function $g_H^S(k, \bar{\rho}, \bar{\rho}')$ are usually only needed for a small set of points $\bar{\rho}$ and $\bar{\rho}'$ since the Neumann boundary conditions on ∂S have been satisfied.

2.1.5. Summary Procedure for Computing $g_H^S(k, \bar{\rho}, \bar{\rho}')$

In summary, the steps in the procedure as follows:

Step 1: At a single low wavenumber k_L^Ω , calculate the impedance matrix elements of P_{mn} of Equation (12) as given in Appendix A.

Step 2: Use Equation (18) to solve for eigenmodes $\psi_\beta^S(\bar{\rho})$ and resonant wavenumbers k_β^S .

Step 3: The normalization of modes $\psi_\beta^S(\bar{\rho})$ are performed by Equations (27) and (28).

Step 4: At a single low wavenumber k_L^S , solve MoM equations for L-shaped waveguide to get $g_H^S(k_L^S, \bar{\rho}, \bar{\rho}')$. Decompose into primary and response as in (29).

Step 5: Construct broadband Green's function $g_H^S(k, \bar{\rho}, \bar{\rho}')$ using low wavenumber extraction of $g_H^S(k_L^S, \bar{\rho}, \bar{\rho}')$, and normalized modal solutions $\psi_\beta^S(\bar{\rho})$ as in Equation (30).

The response Green's function, $g_{HR}^S(k, \bar{\rho}, \bar{\rho}')$ is given by subtracting the primary at k

$$g_{HR}^S(k, \bar{\rho}, \bar{\rho}') = g_0(k_L^S, \bar{\rho}, \bar{\rho}') + g_{HR}^S(k_L^S, \bar{\rho}, \bar{\rho}') - g_0(k, \bar{\rho}, \bar{\rho}') + \sum_\beta \frac{k^2 - (k_L^S)^2}{\left((k_\beta^S)^2 - k^2\right) \left((k_\beta^S)^2 - (k_L^S)^2\right)} \psi_\beta^S(\bar{\rho}) \psi_\beta^S(\bar{\rho}') \quad (31)$$

The procedure thus includes one MoM solution at low wavenumber k_L^S for arbitrarily shaped waveguide (L-shaped waveguide). The result in Equation (31) is labelled as broadband because the dependence on frequency/wavenumber is merely in the factor $\frac{(k^2 - (k_L^S)^2)}{((k_\beta^S)^2 - k^2)}$ while the rest of the expression is independent of wavenumber/frequency.

The method of DC extraction is used in BI-RME [8] for the cases of rectangular waveguide and circular waveguide. In such cases, closed form analytical expressions were obtained for the DC extraction. The DC extraction offers only a small advantage for rectangular and circular waveguides. Analytical expressions of DC extraction have not been derived for arbitrary shape waveguide S . At frequency in the GHz range, we find it convenient to use low wavenumber extraction because the method is general and can be implemented numerically for rectangular, circular and arbitrary shape waveguides rather than relying on closed form analytical expressions. Another reason is because the DC extraction method needs to deal with the mode at $k_{mn} = 0$ for arbitrary shape waveguide, while low wavenumber extraction circumvents the problem. We also use a modal series representation in the Appendix for low wavenumber extraction of the rectangular waveguide.

It is to be noted that the BIRME [8] had not been used to construct the Green's function for the arbitrary waveguide. In this paper, we use the modes of arbitrary waveguide to construct the broadband Green's function (BBGFL). We next apply the method of BBGFL for broadband simulations of the multiple vias problem.

2.2. Application of Broadband Green's Function of Arbitrary Waveguide to Foldy Lax Multiple Scattering Equation for Scattering by Vertical Vias

We next consider multiple vias in the arbitrary shaped waveguide S . The Green's function at an arbitrary k can be separated into the primary Green's function and the wall Green's function $g_W^S(k, \bar{\rho}, \bar{\rho}')$. The wall Green's function is the same as the response Green's function $g_{HR}^S(k, \bar{\rho}, \bar{\rho}')$ of Equation (31). We used the name wall Green's function next to be consistent with the previous

paper in which we combined MoM with the Foldy Lax equation [11]. In this section, we combine the BBGFL with Foldy Lax multiple scattering solutions.

We treat the TM modes with

$$k_{zl} = \frac{l\pi}{d}; \quad k_{\rho l} = \sqrt{k^2 - k_{zl}^2} \quad (32)$$

where $l = 0, 1, 2, \dots$. The separation between the two plates is d , and k is the wavenumber. In the problem of PCB power/ground plane pair, $kd \ll 1$. Thus modes with $l \neq 0$ are evanescent and will not propagate to the wall and have little reflection from the boundary walls. We include the boundary effects of the waveguide for the $l = 0$ mode. The modes with $l \neq 0$ are included in the results but follow the treatment of Foldy Lax equations as that of infinite ground plane [17–19]. In the $l \neq 0$ modes, the near field interactions are included among the vias and between the antipad source and the vias. For TM_0 mode, the electric field only has the E_z component which is represented by the wave function ψ . The “ z ” subscript in E_z will be suppressed. For the $l = 0$ mode, $k_{zl} = 0$ and $k_{\rho l} = k$. Since there is no variation with z ; we use only the 2-dimensional del operator ∇_t and the two dimensional position vector $\bar{\rho}$. The power/ground planes have perfect magnetic conductor (PMC) on the boundary walls. Thus the wave functions obey Neumann boundary conditions.

In the following we suppress the k dependence in g_W and g_0 , since in solving Foldy Lax equations, we solve the equations for each k .

Consider a via centered at $\bar{\rho}_p$ (left circle in Figure 3). From the via, the E_z component of the outgoing m th cylindrical wave of the TM_0 mode is

$$E_m(\bar{\rho} - \bar{\rho}_p) = k H_m^{(2)}(k|\bar{\rho} - \bar{\rho}_p|) e^{-jm\phi_{\bar{\rho}\bar{\rho}_p}} \quad (33)$$

where $\phi_{\bar{\rho}\bar{\rho}_p}$ is the angle between the vector $\bar{\rho} - \bar{\rho}_p$ and the x axis. To obtain $E_m(\bar{\rho} - \bar{\rho}_p)$ from $g_0(\bar{\rho}, \bar{\rho}_a)$, we use the relation

$$g_0(\bar{\rho}, \bar{\rho}_a) = \frac{1}{4j} H_0^{(2)}(k|\bar{\rho} - \bar{\rho}_a|) = \sum_m \frac{1}{4jk} J_m(k|\bar{\rho}_a - \bar{\rho}_p|) \exp(jm\phi_{\bar{\rho}_a\bar{\rho}_p}) E_m(\bar{\rho} - \bar{\rho}_p) \quad (34)$$

Consider $\bar{\rho}_a$ to be points on a circular cylinder of radius R_1 about the via center $\bar{\rho}_p$ (left circle in Figure 3). Then

$$E_m(\bar{\rho} - \bar{\rho}_p) = \frac{4jk}{2\pi J_m(kR_1)} \int_0^{2\pi} d\phi_{\bar{\rho}_a\bar{\rho}_p} \exp(-jm\phi_{\bar{\rho}_a\bar{\rho}_p}) g_0(\bar{\rho}, \bar{\rho}_a) \quad (35)$$

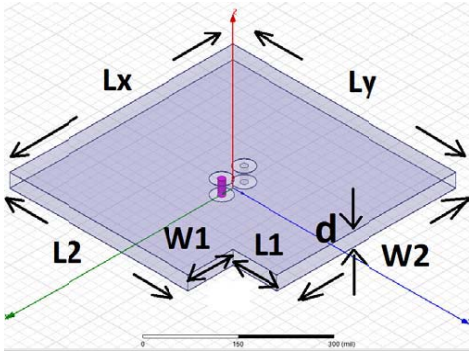


Figure 2. 3D geometry of the L-shaped power/ground plane pair with small cut out and 2 vias.

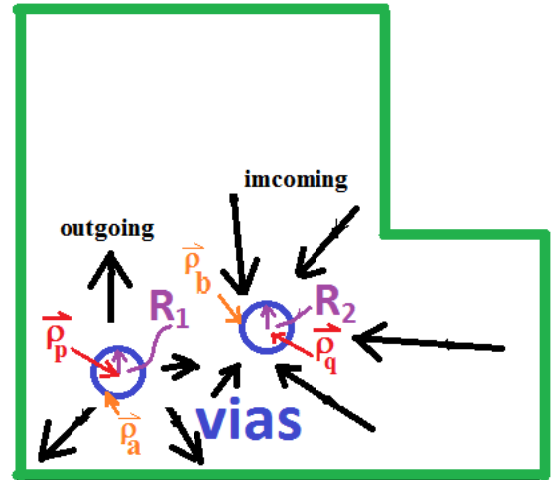


Figure 3. Calculation of X_{nm}^{qpW} by integration over two circles of radii R_1 and R_2 around $\bar{\rho}_p$ and $\bar{\rho}_q$ respectively.

The electric field of the m th cylindrical wave from via p is incident on the wall. The scattered field from the wall, $E_s^{Wpm}(\bar{\rho})$, is expressed in terms of the wall Green's function $g_W(\bar{\rho}, \bar{\rho}_a)$.

$$E_s^{Wpm}(\bar{\rho}) = \frac{4jk}{2\pi J_m(kR_1)} \int_0^{2\pi} d\phi_{\bar{\rho}_a \bar{\rho}_p} \exp(-jm\phi_{\bar{\rho}_a \bar{\rho}_p}) g_W(\bar{\rho}, \bar{\rho}_a) \quad (36)$$

Next, we consider the wall reflected field $E_s^{Wpm}(\bar{\rho})$ to be incident on via q . The via q can be the same via, in which case, $q = p$, or not the same via, in which case, $q \neq p$. The scattered field from the wall onto via q is expanded in regular wave functions, $RgE_n(\bar{\rho} - \bar{\rho}_q)$, about via q

$$E_s^{Wpm}(\bar{\rho}) = \sum_n RgE_n(\bar{\rho} - \bar{\rho}_q) X_{nm}^{qpW} \quad (37)$$

where

$$RgE_n(\bar{\rho} - \bar{\rho}_q) = kJ_n(k|\bar{\rho} - \bar{\rho}_q|) \exp(-jn\phi_{\bar{\rho} \bar{\rho}_q}) \quad (38)$$

In (37), X_{nm}^{qpW} is the coefficient, due to the wall reflection, that couples the m th cylindrical outgoing wave of via p to the n th incident cylindrical wave onto via q . The X_{nm}^{qpW} coefficients are obtained by

$$X_{nm}^{qpW} = \frac{1}{2\pi k J_n(kR_2)} \int_0^{2\pi} d\phi_{\bar{\rho}_b \bar{\rho}_q} \exp(jn\phi_{\bar{\rho}_b \bar{\rho}_q}) E_s^{Wpm}(\bar{\rho}_b) \quad (39)$$

where $\bar{\rho}_b$ are points on a circular cylinder of radius R_2 about the via $\bar{\rho}_q$ (right circle in Figure 3). Substituting (36) into (39),

$$X_{nm}^{qpW} = \frac{1}{2\pi k J_n(kR_2)} \int_0^{2\pi} d\phi_{\bar{\rho}_b \bar{\rho}_q} \exp(jn\phi_{\bar{\rho}_b \bar{\rho}_q}) \frac{4jk}{2\pi J_m(kR_1)} \int_0^{2\pi} d\phi_{\bar{\rho}_a \bar{\rho}_p} \exp(-jm\phi_{\bar{\rho}_a \bar{\rho}_p}) g_W(\bar{\rho}_b, \bar{\rho}_a) \quad (40)$$

The above equation calculates X_{nm}^{qpW} in terms of the wall Green's function $g_W(\bar{\rho}_b, \bar{\rho}_a)$ by carrying out integrations over two circles (left and right circles in Figure 3). In our previous paper [11] combining MoM with Foldy-Lax multiple scattering, the coefficients X_{nm}^{qpW} were obtained by solving the surface integral equation of MoM for each wavenumber k . After the X_{nm}^{qpW} coefficients are obtained, the Foldy Lax equations of multiple scattering in the presence of the wall can be solved [11]. We use matrix notations. The dimension is $(2M+1)$, $n = -M, -(M-1), \dots, (M-1), M$, where M is the maximum harmonic index. Let superscript t be used to denote the transpose. Then

$$\bar{E}^t(\bar{\rho} - \bar{\rho}_q) = [E_{-M}(\bar{\rho} - \bar{\rho}_q) \ E_{-(M-1)}(\bar{\rho} - \bar{\rho}_q) \ \dots \ E_M(\bar{\rho} - \bar{\rho}_q)] \quad (41)$$

Let $\bar{\bar{X}}^{qpW}$ be a matrix of dimension $(2M+1) \times (2M+1)$. Consider N vias in the waveguide. The via index is q , $q = 1, 2, 3, \dots, N$.

The T -matrix coefficients. in the absence of the wall, are

$$T_m = -\frac{J_m(ka)}{H_m^{(2)}(ka)}; \quad m = 0, \pm 1, \dots, \pm M \quad (42)$$

In matrix notations, the T matrix in the absence of the wall, $\bar{\bar{T}}^q$, is a $(2M+1) \times (2M+1)$ diagonal matrix, with diagonal element equal to T_m . Let $\bar{\bar{\tau}}^q$ be the T -matrix of the q th via, $q = 1, 2, \dots, N$, including the wall effect. It is calculated by

$$\bar{\bar{\tau}}^q = \left(\bar{\bar{I}} - \bar{\bar{T}}^q \bar{\bar{X}}^{qqW} \right)^{-1} \bar{\bar{T}}^q \quad (43)$$

where $\bar{\bar{\tau}}^q$ relates \bar{A}^q , the scattered coefficient of via q , to the \bar{w}^q , the exciting coefficient on via q by

$$\bar{A}^q = \bar{\bar{\tau}}^q \bar{w}^q \quad (44)$$

\bar{A}^q and \bar{w}^q are both of dimensions $(2M+1) \times 1$.

Using the scattered field coefficients, \bar{A}^q and the $\bar{\bar{\tau}}^q$, we have the Foldy Lax multiple scattering equations

$$\bar{w}^q = \bar{a}^{q,inc} + \sum_{p \neq q}^N \left[\bar{\bar{\alpha}}_{qp}^+ + \bar{\bar{X}}^{qpW} \right] \bar{A}^p \quad (45)$$

where the nm element of the matrix $\overline{\overline{\alpha}}_{qp}^+$ is

$$\left[\overline{\overline{\alpha}}_{qp}^+\right]_{nm} = H_{n-m}^{(2)}(k|\bar{\rho}_p - \bar{\rho}_q|) e^{j(n-m)\phi_{\bar{\rho}_p\bar{\rho}_q}} \quad (46)$$

$\overline{\overline{\alpha}}_{qp}^+$ is of dimension $(2M+1) \times (2M+1)$.

Substituting (44) into (45), the Foldy Lax multiple scattering equations are

$$\bar{w}^q = \bar{a}^{q,inc} + \sum_{p \neq q}^N \left[\overline{\overline{\alpha}}_{qp}^+ + \overline{\overline{X}}^{qpW} \right] \overline{\overline{\tau}}^p \bar{w}^p \quad (47)$$

where $\bar{a}^{q,inc}$ are the incident field coefficients for sources on the antipad [9, 12, 18, 19].

In summary, the procedure of modeling of vias in arbitrarily shaped power/ground planes using BBGFL and Foldy-lax equation is as follows.

Step 1: solve the broadband wall Green's function $g_W^S(k, \bar{\rho}, \bar{\rho}')$ for the cavity structure of power/ground planes using BBGFL as described in the previous section.

Step 2: calculates X_{nm}^{qpW} by Equation (40) using values of the wall Green's function $g_W(\bar{\rho}_b, \bar{\rho}_a)$ on the circles in Figure 3.

Step 3: solve the $\overline{\overline{\tau}}^q$ matrix for each via $q = 1, \dots, N$ by Equation (43) using $\overline{\overline{X}}^{qpW}$.

Step 4: solve the combined problem of vias and power/ground planes using Foldy-Lax multiple scattering Equation (47).

Step 5: after the Foldy-Lax multiple scattering equations are solved, we then follow the equations given in [11] to calculate the currents on the vias. The admittance matrices and the scattering matrices are then calculated as in [9, 17].

3. NUMERICAL RESULTS

The L-shaped waveguide in Figure 1(b) is used. The dimension parameters are: $Lx = Ly = 500$ mils, $L1 = 250$ mils, and $W1 = 100$ mils. We show first the results of resonance wavenumber and the eigenmodes. Then, we show the results of the Green's functions. The dependence of the broadband Green's function on frequency and materials properties are through $k^2 = \omega^2 \mu_0 \varepsilon_0 \varepsilon_r$ where ε_r is the relative permittivity. We only need to specify k for the modal solution and the Green's functions.

In calculating the field solution of the modal solutions and the Green's function, the field points are located at $y = 20$ mils, $x = [-245 \text{ mils}, 245 \text{ mils}]$ and the source point is located at (25 mils, 20 mils).

Table 1. Comparison of MoM and BBGFL for resonant frequencies of Neumann case.

MoM Mode Number	MoM resonant wave number in inverse meter	BBGFL Mode Number Total/physical	BBGFL resonant wave number In inverse meter
0 (constant mode)	2.638	0 (constant mode)	0
1	229.5	1/1	228.7
2	277.0	2/2	276.9
3	371.5	3/3	371.7
4	495.0	4/4	494.8
5	513.9	5/5	513.7
6	561.8	6/6	561.3
7	641.0	7/7	646.0
8	674.4	8/8	661.2
NA	NA	9/NA	674.2 (nonphysical mode)
9	750.9	10/9	750.6
10	757.5	11/10	757.5

We compare the results with that of MoM. In calculating resonant wavenumber and resonant mode with MoM, we set up the integral equation using the free space Green's function $g_0(k, \bar{\rho}, \bar{\rho}') = H_0^{(2)}(k|\bar{\rho} - \bar{\rho}'|)/(4j)$. We then search the values of real k that obey the surface integral equation.

3.1. Computation of Green's Functions for Neumann Case

3.1.1. Resonant Wavenumber Comparison

In Table 1, we compare the resonant wavenumbers k as computed by BBGFL and MoM. The eigenmatrix equation of the present approach can give nonphysical modes in addition to physical modes. The nonphysical modes can be quickly identified because the eigenfunction of a physical mode, for the Neumann case, is constant outside the original solution boundary. In Table 1, there is 1 nonphysical mode (the 9th mode) in the BBGFL solution. Thus the 9th mode of MoM is compared with the 10th mode of BBGFL. Results in Table 1 show that BBGFL and MoM are in good agreement.

3.1.2. Comparisons of Modal Solutions

In the BBGFL, the eigenmatrix equations and the resonant wavenumbers are real. Thus the modal solutions are real. On the other hand, in using MoM to calculate the modes, the Hankel function is

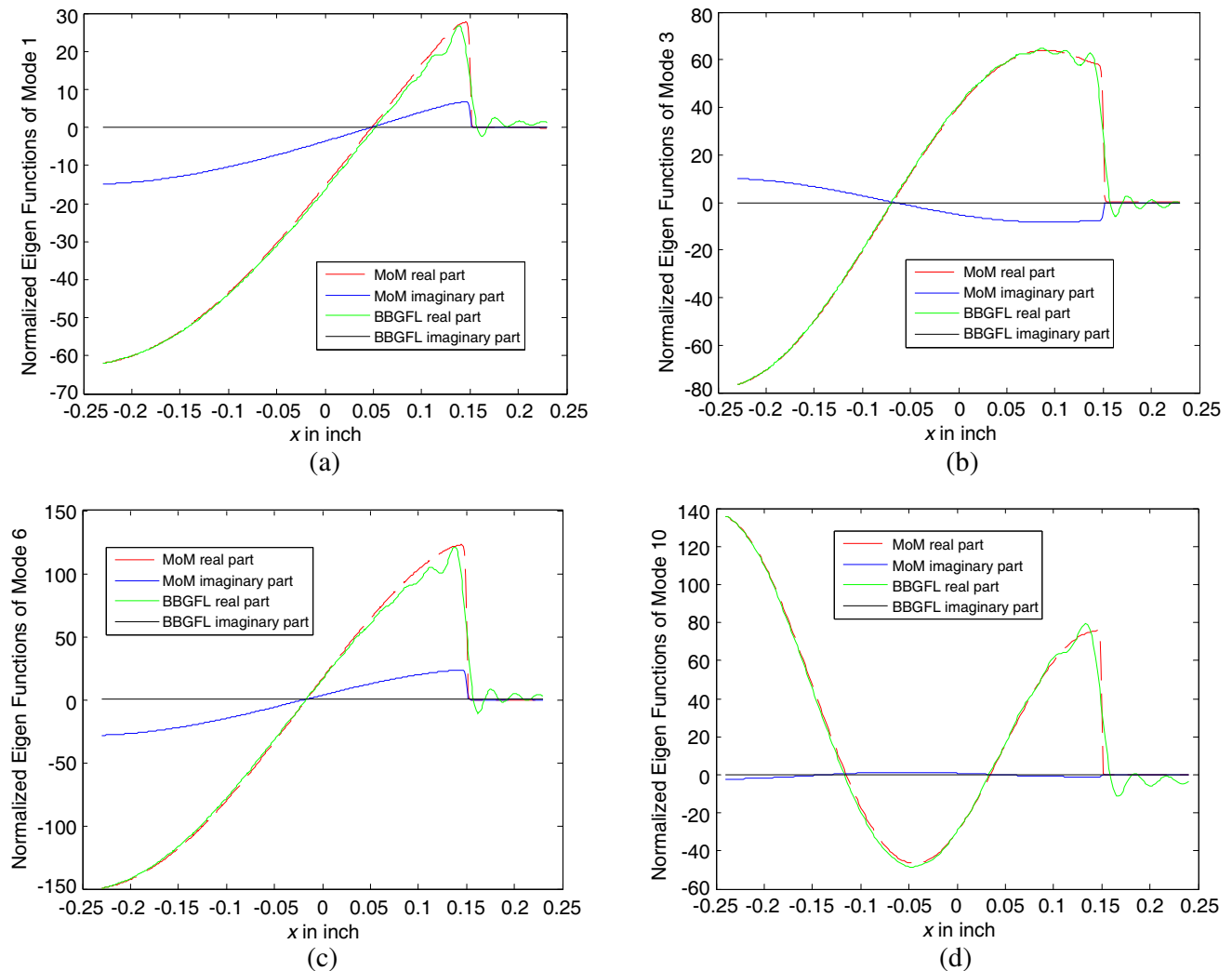


Figure 4. Comparison of MoM and BBGFL for modal solutions of Neumann case. (a) Mode #1 at $k = 228.7$, (b) Mode #3 at $k = 371.7$, (c) Mode #6 at $k = 561.3$, (d) Mode #10 at $k = 575.5$.

complex. Thus the MoM results have small imaginary parts in the solutions depending on the accuracy of the nonlinear search in applying MoM. In Figure 4, we compare the modal solutions of BBGFL and MoM. The eigen functions from MoM are normalized to the same scale as BBGFL. Four of the modes listed in Table 1 are compared. Results are in good agreement.

3.1.3. Comparisons of Green's Function g_H^S

In Figure 5, we compare the Green's function computed by BBGFL and MoM for various real wavenumbers k . In the low wavenumber extractions, we use $k_L^\Omega = 0.044$, and $k_L^S = 220$. The results of BBGFL and MoM are in good agreement.

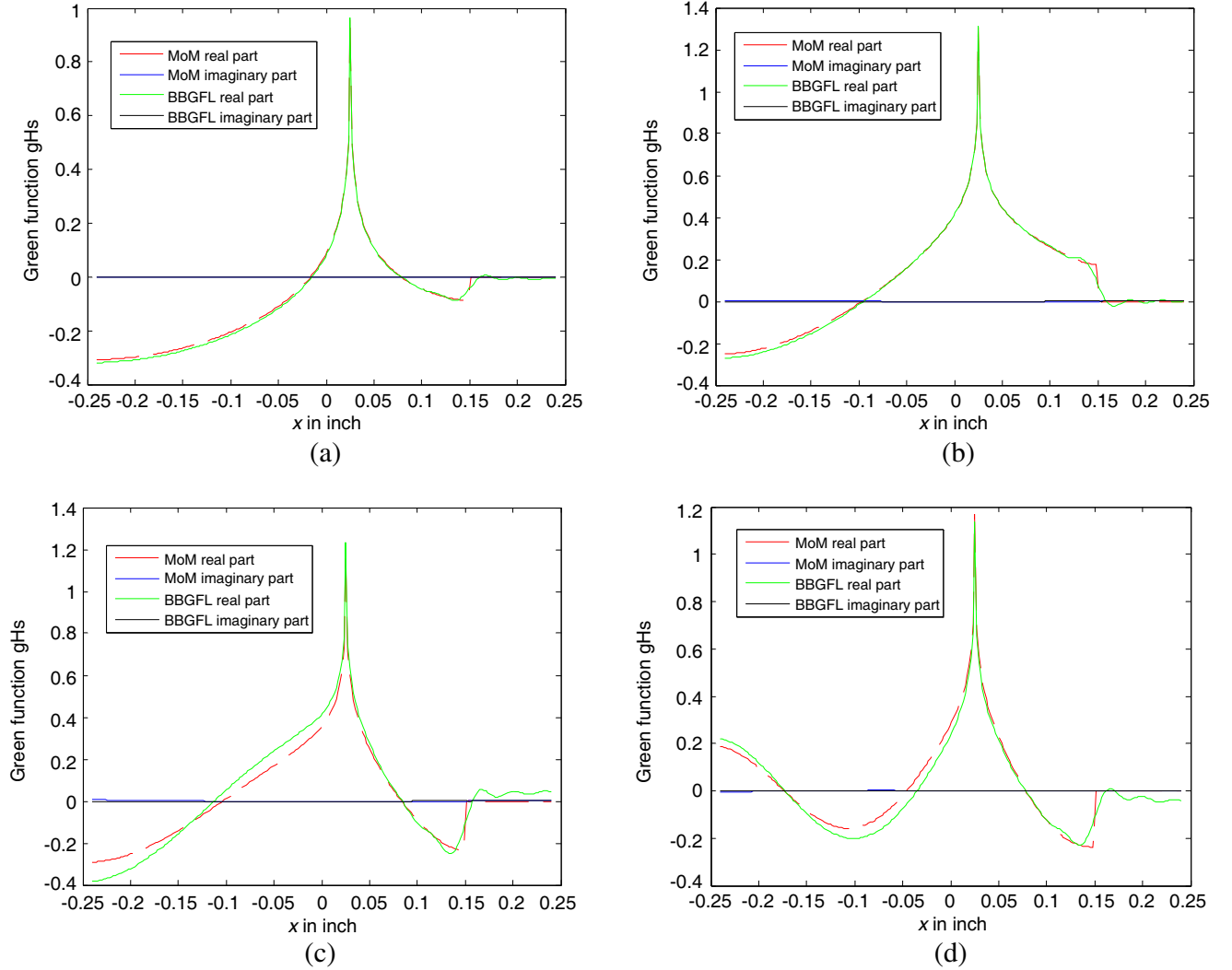


Figure 5. Comparison between MoM and BBGFL for Green's function of Neumann case. (a) Neumann gHs at $k = 175.8$, (b) Neumann gHs at $k = 351.7$, (c) Neumann gHs at $k = 615.5$, (d) Neumann gHs at $k = 879.2$.

3.1.4. Comparisons of CPU Times

In Table 2, we compare the CPU times of BBGFL and MoM for computing the Green's function. In the comparisons, the input simulation parameters are: the discretization spacing is 2 mils for both MoM and BBGFL, the BBGFL uses $M_o = 30$ for both kxm and kyn with total $M_\alpha = (1 + M_o) \times (1 + M_o) = 961$

Table 2. Comparison of BBGFL and direct MoM for CPU times.

Methods	1 wavenumber point	10 wavenumber points
BBGFL	$40.28\text{ s} + 0.18 = 40.46\text{ sec}$	$40.28\text{ s} + 0.18 * 10 = 42.08\text{ sec}$
Direct MoM	36.01 sec	$36.01 * 10 = 360.1\text{ sec}$
Methods	100 wavenumber points	1000 wavenumber points
BBGFL	$40.28\text{ s} + 0.18 * 100 = 58.28\text{ sec}$	$40.28\text{ s} + 0.18 * 1000 = 220.28\text{ sec}$
Direct MoM	$36.01 * 100 = 3601\text{ sec}$	$36.01 * 1000 = 36010\text{ sec}$

modes. For each frequency point, the Green's function is calculated with 1 source point and 240 observation points. Note, for BBGFL, the CPU time consists two parts: the first part is for computing eigenfunctions and eigenvalues, and second part is to calculate Green's function with the computed eigenfunctions and eigenvalues. In the Table 2, for 1000 wavenumber points, the first part takes 40.28 seconds, while the second part is only 180 seconds for computing the g_H of 240 observation points. This indicates that, even for computation of 240 observation points, the CPU of second part is still negligible. For broadband modeling with 1000 wavenumber points, the proposed method is more than 162 times faster than MoM. The Green's functions are at many wavenumber points. In this problem, the method of calculating a few wavenumber points followed by interpolation at other wavenumber points, is not accurate because of the multiple resonances.

3.2. Application of BBGFL to the Simulation of Vias in Arbitrarily Shaped PCB Power/Ground Plane Pair

We next model the scattering matrices for the problem of multiple vias in the L-shaped PCB/power ground plane for the frequency range up to 20 GHz. The dielectric thickness d between the two parallel plates is 30 mils. Thus $kd \ll 1$. For the sake of simplicity in combining BBGFL with the Foldy Lax approach, we only use the zeroth harmonic for the $l = 0$ mode in the Foldy Lax approach. We included higher order harmonics for $l > 0$ modes.

3.2.1. Modeling of Two Signal Vias in a Rectangular Power/Ground Plane Pair with Small Cut Out

Consider a power/ground plane pair with two signal vias as showed in Figure 2. $Lx = Ly = 500$ mils, $L1 = 100$ mils, $W1 = 100$ mils. The relative permittivity is complex and is set at $\epsilon_r = 3.4(1 - j0.02)$. Vias 1 and 2 are located at $(-25, 0)$ mil and $(25, 0)$ mil, respectively. Using notations as in Reference [12, 19], the via radius is $a = 6.75$ mils, and the antipad radius is $b = 20$ mils.

In Figure 6, we compare the results of the 4 methods for the S -parameters of insertion loss, return loss, near end crosstalk (NEXT), and far end crosstalk (FEXT). The red curves are results obtained by using BBGFL with Foldy-Lax. The blue curves are results from HFSS. We also consider the case with $\ell = 0$ only and also the case with higher order $\ell \geq 1$ included. The green curves are results from direct MoM solution with signal vias and plane pair, with $\ell = 0$ mode. Direct MoM means solving, at every frequency, the surface integral equation of arbitrary ground plane and vias formulated with free space Green's function. The black curves are results combining direct MoM solution with $\ell = 0$ mode, and Foldy-Lax solution with $\ell \geq 1$ modes. The results of BBGFL/Foldy-Lax (red) are in good agreement with HFSS (blue) and MoM/Foldy-Lax (black). It can be seen that all the methods capture the resonance frequencies, which are caused by the reflections by the PMC walls of the finite power/ground plane. However, the green results with only $\ell = 0$ has large difference compared to other methods. This means the $\ell > 0$ modes are important for the coupling effects caused by the dense vias (small pitch between two vias). Because the vias are small and are not near the boundary, the $(n, m) = (0, 0)$ in the wall coupling coefficients X_{nm}^{qpW} has the dominant effects. In our simulations, we used $R_1 = R_2 = a$ (Figure 3).

3.2.2. Modeling of Two Signal Vias in a Rectangular Power/Ground Plane Pair with Large Cut Out

Consider a power/ground plane pair with two signal vias as showed in Figure 2. $Lx = Ly = 500$ mils, $L1 = 100$ mils, $W1 = 200$ mils. The relative permittivity is real and is $\epsilon_r = 3.4$. Vias 1 and 2 are located at $(-25, 0)$ mil and $(25, 0)$ mil, respectively. The via radius is 6.75 mils, and the antipad radius is 20 mils.

In Figure 7, BBGFL is compared with three different methods. The results of the S -parameters of insertion loss, return loss, near end crosstalk (NEXT), and far end crosstalk (FEXT) are shown. The red curves are results obtained by using BBGFL with Foldy-Lax. The blue curves are results from HFSS. The green curves are results from direct MoM solution with $\ell = 0$ mode. The black curves are results combining direct MoM solution with $\ell = 0$ mode, and Foldy-Lax solution with $\ell > 0$ modes. The BBGFL/Foldy-Lax (red) results are in good agreement with HFSS (blue) and MoM/Foldy-Lax (black). It can be seen that all the methods can capture the resonance frequencies, which are caused by reflections from the walls of the finite plane. The results also show that higher order modes $\ell > 0$ modes are important.

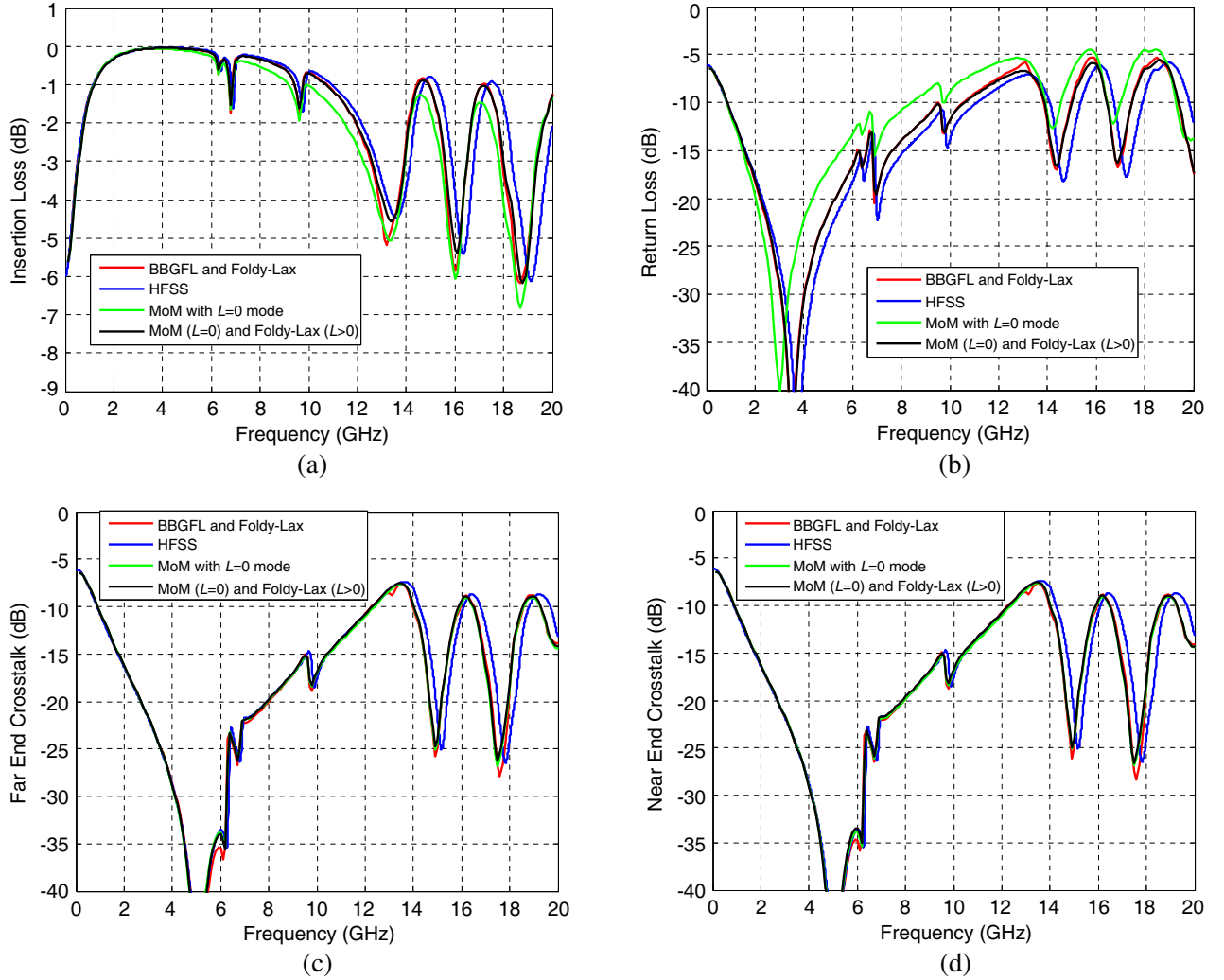


Figure 6. Comparison of BBGFL and different methods for S -parameters from simulations with Figure 2: Red — BBGFL/Foldy-Lax, Blue — HFSS, Green — direct MoM with $L = 0$ mode, Black — combine direct MoM with $L = 0$ mode and Foldy-Lax with $L > 0$ modes. (a) Insertion Loss, (b) Return Loss, (c) Far End Crosstalk, (d) Near End Crosstalk.

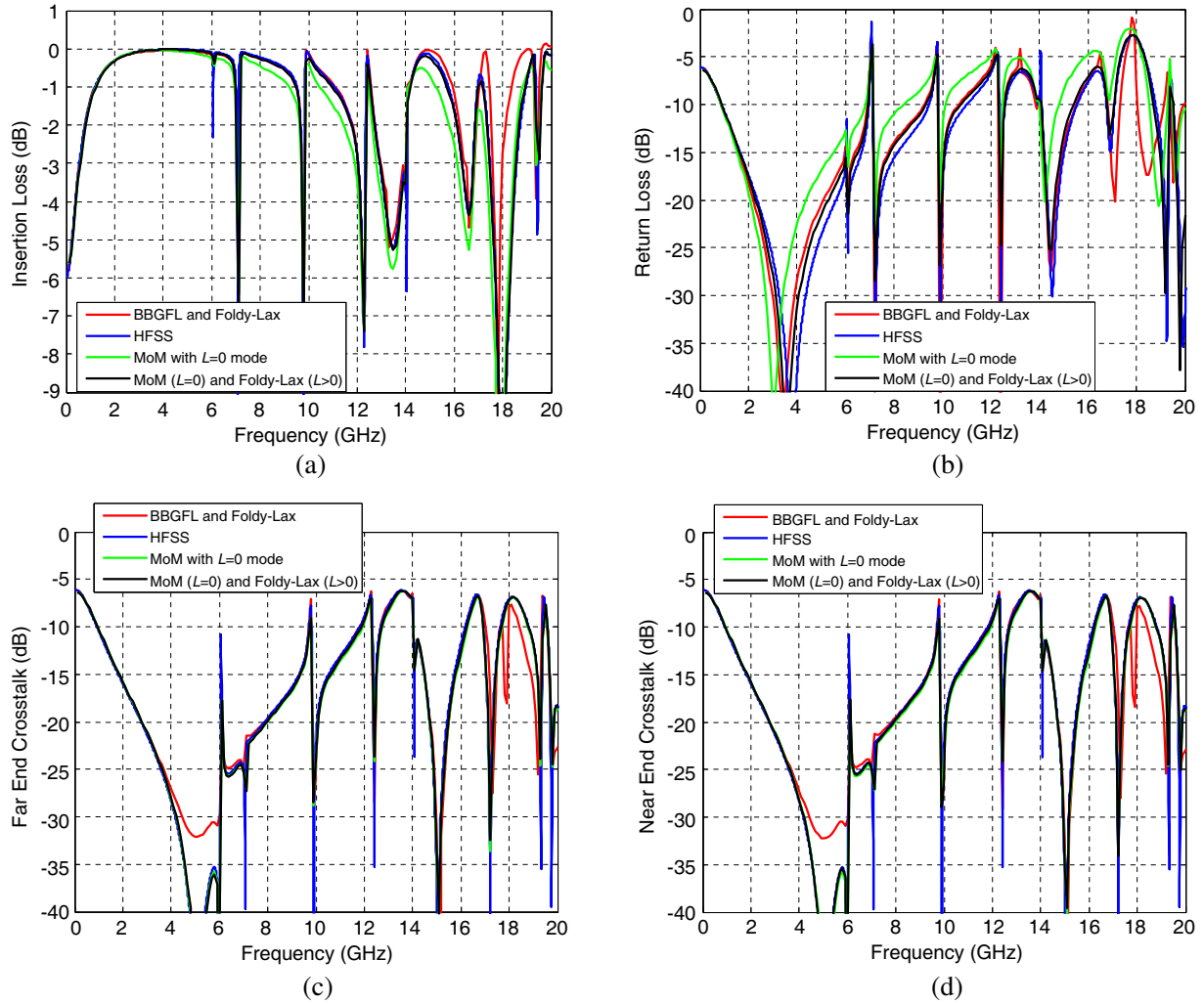


Figure 7. Comparison of BBGFL and different methods for S -parameters: Red — BBGFL/Foldy-Lax, Blue — HFSS, Green — direct MoM with $L = 0$ mode, Black — combine direct MoM with $L = 0$ mode and Foldy-Lax with $L > 0$ modes. (a) Insertion Loss, (b) Return Loss, (c) Far End Crosstalk, (d) Near End Crosstalk.

3.2.3. Modeling of Two Signal Vias and Two Shorting Vias in a Rectangular Power/Power (or Ground/Ground) Plane Pair with Large Cut Out

Consider a power/power or ground/ground plane pair with two signal vias and two shorting vias as shown in Figure 8. The parameters are $Lx = Ly = 500$ mils, $L1 = 200$ mils, $W1 = 100$ mils. The relative permittivity is $\epsilon_r = 3.4(1 - j0.02)$. Vias 1 and 2 are signal vias, and they are located at $(-25, 0)$ mil and $(25, 0)$ mil respectively. The two shorting vias are located at $(0, -25)$ mil and $(0, 25)$ mil, respectively. The via radius is 6.75 mils, and the antipad radius is 20 mils.

In Figure 9, the S -parameters of insertion loss, return loss, near end crosstalk (NEXT), and far end crosstalk (FEXT) are shown. The results are in good agreement.

3.2.4. Modeling of 8 Vias: Four Signal Vias and Four Shorting Vias in a Rectangular Power/Power (or Ground/Ground) Plane Pair with Large Cut Out

Next, we consider a larger number of vias. Consider a power/power or ground/ground plane pair with 4 signal vias and 4 shorting vias as showed in Figure 10. The parameters are $Lx = Ly = 500$ mils, $L1 = 200$ mils, $W1 = 100$ mils. The relative permittivity is $\epsilon_r = 3.4(1 - j0.02)$. Signal Vias 1, 2, 3

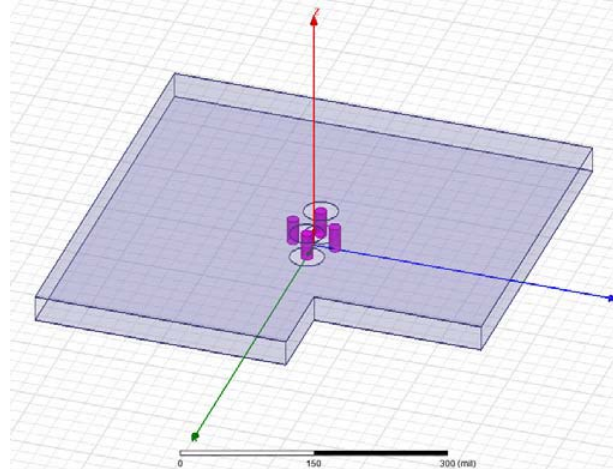


Figure 8. 3D geometry of the simulation with 2 signal vias and 2 shorting vias in an irregular shaped plate pair with large cut out.

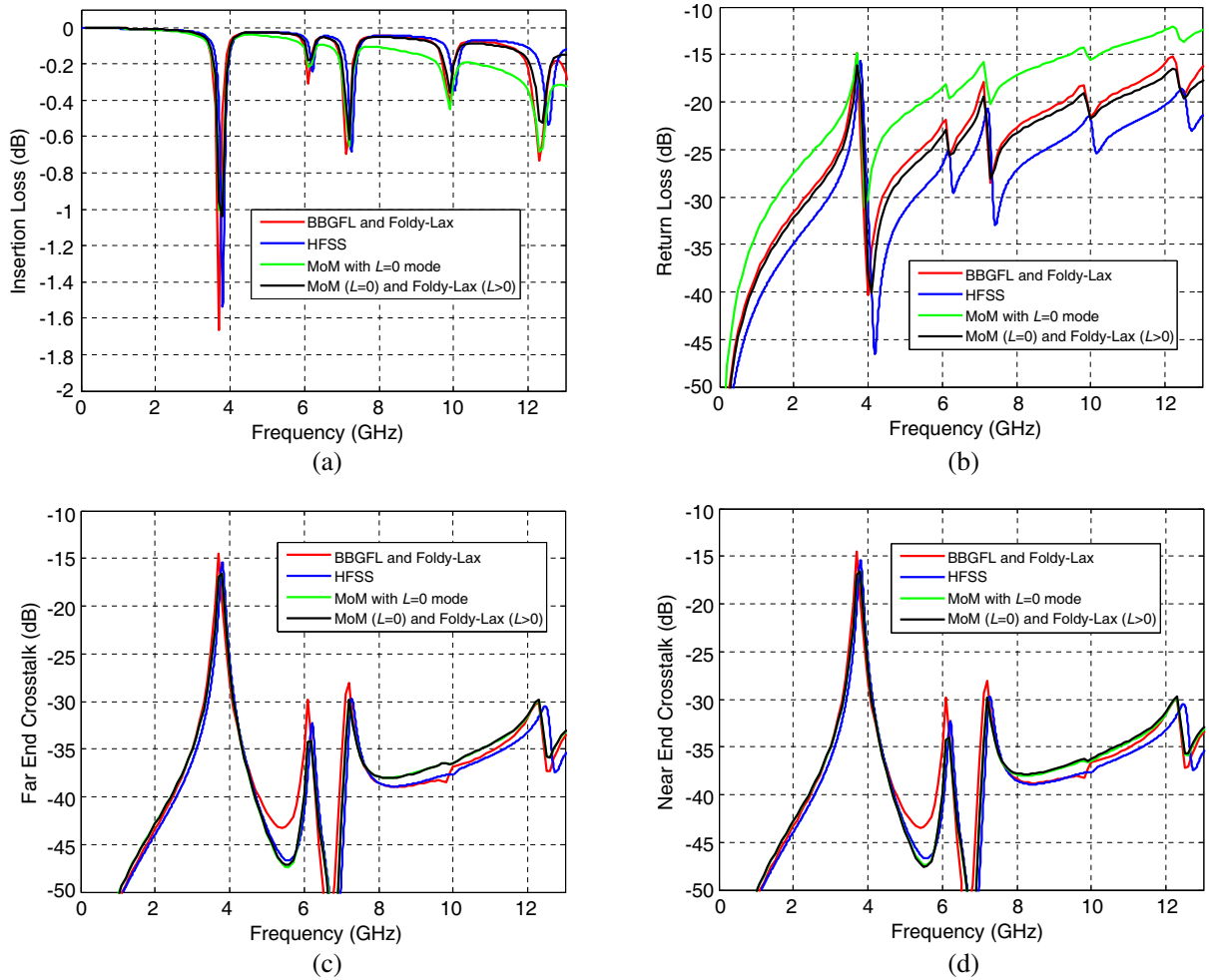


Figure 9. Comparison of BBGFL and different methods for s-parameters from simulations with Figure 8: Red — BBGFL/Foldy-Lax, Blue — HFSS, Green — direct MoM with $L = 0$ mode, Black — combine direct MoM with $L = 0$ mode and Foldy-Lax with $L > 0$ modes. (a) Insertion Loss, (b) Return Loss, (c) Far End Crosstalk, (d) Near End Crosstalk.

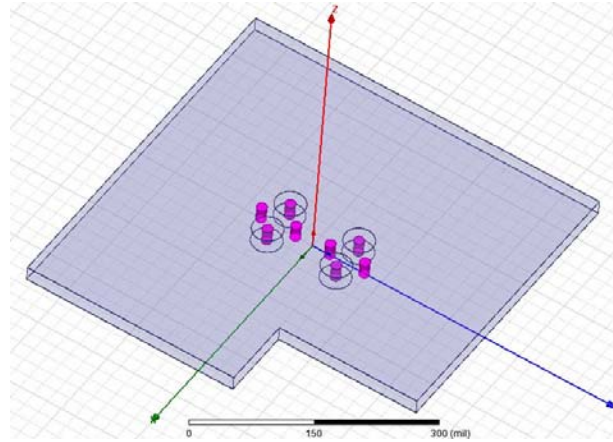


Figure 10. 3D geometry of the simulation with 4 signal vias and 4 shorting vias in an irregular shaped plate pair with large cut out.

and 4 are located at $(-25, 50)$, $(25, 50)$, $(-25, -50)$, and $(25, -50)$ mils, respectively. Shorting vias are located at $(0, 75)$, $(0, 25)$, $(0, -25)$, and $(0, -75)$ mils, respectively. Two shorting vias are located at $(0, -25)$ mil and $(0, 25)$ mil, respectively. The via radius is 6.75 mils, and the antipad radius is 20 mils. The results are shown in Figure 11.

The results from the various methods are in good agreement.

3.2.5. Comparisons of CPU Time for Vias Simulations

In Table 3, we compare the CPU time used in the simulations of Figure 8. In the comparisons, the input parameters are: the discretization spacing is 4 mils for both MoM and BBGFL, the BBGFL uses $M_o = 20$ for both k_{xm} and k_{yn} . For BBGFL, the CPU time consists three parts. The first part is for computation of eigenfunctions and resonant wavenumbers. The second part is for creating response Green's function with the computed eigenfunctions and resonant wavenumbers. The third part is solve the Foldy-Lax equations with the response Green's function. We show the sum of the CPU of the 3 parts. The CPU time of HFSS contains two parts. The first part is for simulation setup (CAD meshing, etc.) which is done only once, and the second part is for FEM simulation which needs to be repeated for every frequency point. For the simulations of 1000 frequency points, BBGFL takes 4.7 seconds for first part, 2 seconds for the second part, and 5 seconds for the third part. For the total CPU time used for 100 frequency points, the proposed method is 59 times faster than direct MoM, and is 103 times faster than HFSS. For the total CPU time used for 1000 frequency points, the proposed method is 273 times faster than direct MoM, and is 447 times faster than HFSS. This shows that the BBGFL, combined with Foldy-Lax, is much more efficient than MoM and HFSS for broadband simulations. It is to be noted that large number of frequency points are necessary for multiple resonances for the cavity.

Table 3. Comparison of CPU times using different methods: BBGFL/Foldy-Lax, direct MoM, and HFSS.

Methods	1 frequency point	10 frequency points
BBGFL/Foldy-Lax	$4.7 + 0.002 + 0.005 = 4.707$ sec	$4.7 + 0.002 * 10 + 0.005 * 10 = 4.77$ sec
Direct MoM	3.2 sec	$3.2 * 10 = 32$ sec
HFSS	$35 + 5.2 = 40.2$ sec	$35 + 5.2 * 10 = 87$ sec
Methods	100 frequency points	1000 frequency points
BBGFL/Foldy-Lax	$4.7 + 0.002 * 100 + 0.005 * 100 = 5.4$ sec	$4.7 + 0.002 * 1000 + 0.005 * 1000 = 11.7$ sec
Direct MoM	$3.2 * 100 = 320$ sec	$3.2 * 1000 = 3200$ sec
HFSS	$35 + 5.2 * 100 = 555$ sec	$35 + 5.2 * 1000 = 5235$ sec

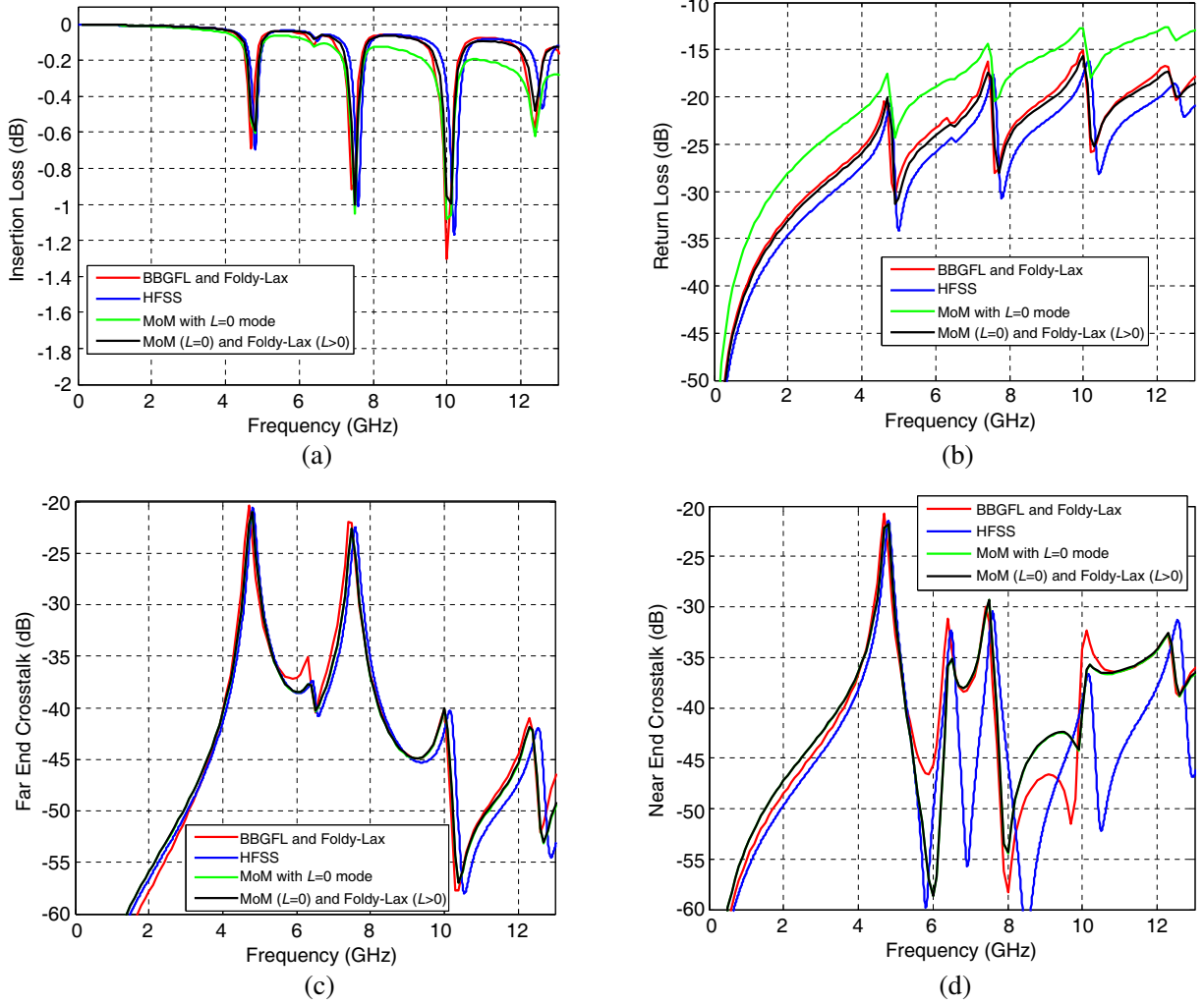


Figure 11. Comparison of BBGFL and different methods for S -parameters from simulations with Figure 10: Red — BBGFL/Foldy-Lax, Blue — HFSS, Green — direct MoM with $L = 0$ mode, Black — combine direct MoM with $L = 0$ mode and Foldy-Lax with $L > 0$ modes. (a) Insertion Loss, (b) Return Loss, (c) Far End Crosstalk, (d) Near End Crosstalk.

4. CONCLUSION

In this paper, we present a new technique, BBGFL, for fast and accurate broadband modeling and simulations of scattering problems in arbitrarily shaped waveguides or cavities. Results show that BBGFL and direct MoM are in good agreement on resonance frequencies, modes, and Green's function. Direct MoM refers to the approach based on free space Green's function that was used in References [10,11]. The proposed method is also implemented for practical PCB applications. We combined BBGFL with Foldy-Lax multiple scattering equation, to simulate vias in arbitrarily shaped power/ground plane pairs. Simulation results show that BBGFL/Foldy-Lax results are in good agreement with MoM and HFSS in S -parameters.

Even including the calculation of modal solutions and the 1-time MoM low wavenumber extraction, the method of BBGFL/Foldy-Lax is still many times faster than direct MoM and HFSS for broadband simulations. We are presently extending the approach to more complicated cases. With fast broadband simulations over a wide frequency range, the results in the time domain can also be obtained from the frequency domain results. We have also implemented the BBGFL with MoM for the vias instead of using Foldy-Lax equations [12, 13]. The case of EMC was also studied [12, 13].

APPENDIX A.

In this appendix, a modal series representation is given for the impedance matrix elements P_{mn} for the non-self-patch and for the self-patch, when the boundary σ consists of straight line segments. Note the calculations of P_{mn} are needed for only a single low wavenumber k_L^Ω .

Let the endpoints of the n th patch be at (x_1, y_1) and (x_2, y_2) . The integration is over the n th patch. The point matching is at the center of the m th patch. Let the slope of the n th patch be s which is a constant for the patch, so that $\frac{y_2 - y_1}{x_2 - x_1} = s$, and $dy = sdx$. Let (x, y) be the field point of point matching and (x', y') be the source point on the patch.

Then on the patch, $y' = s(x' - x_1) + y_1$, $dl' = dx' \sqrt{1 + s^2} = dy' \sqrt{1 + (\frac{1}{s})^2}$, $\Delta t = \Delta x \sqrt{1 + s^2} = \Delta y \sqrt{1 + (\frac{1}{s})^2}$.

If we consider the L-shape case, then $s = 0$, or $s = \infty$ on the two arms of L . The patch integral becomes

$$\begin{aligned} \frac{1}{\Delta t} \int_{\text{patch}} dl' [\hat{n}'_t \cdot \nabla'_t g_H^\Omega(k_L^\Omega, \bar{\rho}')] &= I = \frac{1}{\Delta t} \int dx' \left[-s \frac{\partial}{\partial x'} + \frac{\partial}{\partial y'} \right] g_H^\Omega(k_L^\Omega, \bar{\rho}, \bar{\rho}') \Big|_{y'=s(x'-x_1)+y_1} \\ &= \frac{1}{\Delta t} \sum_{m=0}^{\infty} \sum_{n=0}^{\infty} \frac{A_{mn} A_{mn}}{(k_{mn})^2 - (k_L^\Omega)^2} \cos \frac{m\pi}{L_x} \left(x + \frac{L_x}{2} \right) \cos \frac{n\pi}{L_y} \left(y + \frac{L_y}{2} \right) \\ &\quad \left\{ s \frac{m\pi}{L_x} \int dx' \sin \frac{m\pi}{L_x} \left(x' + \frac{L_x}{2} \right) \cos \frac{n\pi}{L_y} \left(s(x' - x_1) + y_1 + \frac{L_y}{2} \right) \right. \\ &\quad \left. - \frac{n\pi}{L_y} \int dx' \cos \frac{m\pi}{L_x} \left(x' + \frac{L_x}{2} \right) \sin \frac{n\pi}{L_y} \left(s(x' - x_1) + y_1 + \frac{L_y}{2} \right) \right\} \quad (A1) \end{aligned}$$

A.1. Non Self-Patch

Results are

$$\begin{aligned} I &= \frac{1}{\Delta t} \sum_{m=0}^{\infty} \sum_{n=0}^{\infty} \frac{A_{mn} A_{mn}}{(k_{mn})^2 - (k_L^\Omega)^2} \cos \frac{m\pi}{L_x} \left(x + \frac{L_x}{2} \right) \cos \frac{n\pi}{L_y} \left(y + \frac{L_y}{2} \right) \\ &\quad \left\{ s \frac{m\pi}{L_x} \left[\frac{\sin \left(\frac{m\pi}{L_x} \left(\frac{x_1 + x_2}{2} + \frac{L_x}{2} \right) + \frac{n\pi}{L_y} \left(\frac{y_1 + y_2}{2} + \frac{L_y}{2} \right) \right) \sin \left(\frac{m\pi}{L_x} \Delta x + \frac{n\pi}{L_y} \Delta y \right)}{\frac{m\pi}{L_x} + \frac{n\pi}{L_y} s} \right. \right. \\ &\quad \left. - \frac{\sin \left(\frac{m\pi}{L_x} \left(\frac{x_1 + x_2}{2} + \frac{L_x}{2} \right) - \frac{n\pi}{L_y} \left(\frac{y_1 + y_2}{2} + \frac{L_y}{2} \right) \right) \sin \left(\frac{m\pi}{L_x} \Delta x - \frac{n\pi}{L_y} \Delta y \right)}{\frac{m\pi}{L_x} - \frac{n\pi}{L_y} s} \right] \\ &\quad - \frac{n\pi}{L_y} \left[\frac{\sin \left(\frac{n\pi}{L_y} \left(\frac{y_1 + y_2}{2} + \frac{L_y}{2} \right) + \frac{m\pi}{L_x} \left(\frac{x_1 + x_2}{2} + \frac{L_x}{2} \right) \right) \sin \left(\frac{n\pi}{L_y} \Delta y + \frac{m\pi}{L_x} \Delta x \right)}{s \frac{n\pi}{L_y} + \frac{m\pi}{L_x}} \right. \\ &\quad \left. \left. - \frac{\sin \left(\frac{n\pi}{L_y} \left(\frac{y_1 + y_2}{2} + \frac{L_y}{2} \right) - \frac{m\pi}{L_x} \left(\frac{x_1 + x_2}{2} + \frac{L_x}{2} \right) \right) \sin \left(\frac{n\pi}{L_y} \Delta y - \frac{m\pi}{L_x} \Delta x \right)}{s \frac{n\pi}{L_y} - \frac{m\pi}{L_x}} \right] \right\} \quad (A2) \end{aligned}$$

A.2. Self-Patch

Note that in Equation (12a) we only need to calculate the self-patch for the response $g_{HR}^\Omega(k_L^\Omega, \bar{\rho}, \bar{\rho}')$. We divide the self patch into three parts of $\frac{\Delta x}{3}$ each: the left part, the middle part and the right part. The left part and the right part are evaluated directly from the modal series expansion. The middle part is set to be the average of the left part and the right part, making use of the fact that $g_{HR}^\Omega(k_L^\Omega \cdot \bar{\rho}_m, \bar{\rho}')$ is not singular and is smooth on the self-patch

$$\frac{1}{\Delta t} \int_{\text{self-patch}} dl' \hat{n}'_t \cdot \nabla'_t g_{HR}^\Omega(k_L^\Omega, \bar{\rho}, \bar{\rho}') = \frac{3}{2\Delta t} [L + R] \quad (\text{A3})$$

where

$$L = \int_{x_1}^{x_1 + \frac{\Delta x}{3}} dl' \hat{n}'_t \cdot \nabla'_t g_{HR}^\Omega(k_L^\Omega, \bar{\rho}, \bar{\rho}') \quad (\text{A4})$$

$$R = \int_{x_2 - \frac{\Delta x}{3}}^{x_2} dl' \hat{n}'_t \cdot \nabla'_t g_{HR}^\Omega(k_L^\Omega, \bar{\rho}, \bar{\rho}') \quad (\text{A5})$$

In L and R of the self patch, note that $\bar{\rho} \neq \bar{\rho}'$ since the middle part is excluded. On the left part L and the right part R

$$\hat{n}'_t \cdot \nabla'_t g_{HR}^\Omega(k_L^\Omega, \bar{\rho}, \bar{\rho}') = \hat{n}'_t \cdot \nabla'_t g_H^\Omega(k_L^\Omega, \bar{\rho}, \bar{\rho}') - \hat{n}'_t \cdot \nabla'_t g_0(k_L^\Omega, \bar{\rho}, \bar{\rho}') \quad (\text{A6})$$

Since

$$\nabla' g_0(k_L^\Omega, \bar{\rho}, \bar{\rho}') = -\frac{k_L^\Omega}{4j} H_1^{(2)} \left(k_L^\Omega \sqrt{(x' - x)^2 + (y' - y)^2} \right) \hat{t} \quad (\text{A7})$$

where

$$\hat{t} = \hat{x} \frac{(x' - x)}{\sqrt{(x' - x)^2 + (y' - y)^2}} + \hat{y} \frac{(y' - y)}{\sqrt{(x' - x)^2 + (y' - y)^2}} \quad (\text{A8})$$

is the tangential vector on the patch. Thus on L and R ,

$$\hat{n}'_t \cdot \nabla'_t g_0(k_L^\Omega, \bar{\rho}, \bar{\rho}') = 0 \quad (\text{A9})$$

Hence in the integrands of the left part L and right part R ,

$$\hat{n}'_t \cdot \nabla'_t g_{HR}^\Omega(k_L^\Omega, \bar{\rho}, \bar{\rho}') = \hat{n}'_t \cdot \nabla'_t g_H^\Omega(k_L^\Omega, \bar{\rho}, \bar{\rho}') \quad (\text{A10})$$

Thus, using (A2), (A4), (A5) and (A10), L is equal to the expression I of (A2) with the replacements, $x_2 \rightarrow x_1 + \frac{\Delta x}{3}$, $y_2 \rightarrow y_1 + \frac{\Delta y}{3}$, $\Delta x \rightarrow \frac{\Delta x}{3}$, $\Delta y \rightarrow \frac{\Delta y}{3}$. For R , it is equal to the expression I of (A2) with the replacements, $x_1 \rightarrow x_2 - \frac{\Delta x}{3}$, $y_1 \rightarrow y_2 - \frac{\Delta y}{3}$, $\Delta x \rightarrow \frac{\Delta x}{3}$, $\Delta y \rightarrow \frac{\Delta y}{3}$.

REFERENCES

1. Swaminathan, M., D. Chung, S. Grivet-Talocia, K. Bharath, V. Laddha, and J. Xie, "Designing and modeling for power integrity," *IEEE Trans. Electromagn. Compat.*, Vol. 52, No. 2, 288–310, May 2010.
2. Li, E.-P., X.-C. Wei, A. C. Cangellaris, E.-X. Liu, Y.-J. Zhang, M. D'Amore, J. Kim, and T. Sudo, "Progress review of electromagnetic compatibility analysis technologies for packages, printed circuit boards, and novel interconnects," *IEEE Trans. Electromagn. Compat.*, Vol. 52, No. 2, 248–265, May 2010.
3. Leone, M., "The radiation of a rectangular power-bus structure at multiple cavity-mode resonances," *IEEE Trans. on Microw. Theory and Tech.*, Vol. 45, No. 3, 486–492, Aug. 2003.
4. Shim, H.-W. and T. H. Hubing, "A closed-form expression for estimating radiated emissions from the power planes in a populated printed circuit board," *IEEE Trans. Electromagn. Compat.*, Vol. 48, No. 1, 74–81, Feb. 2006.

5. Kim, J.-H. and M. Swaminathan, "Modeling of irregular shaped power distribution planes using transmission matrix method," *IEEE Transactions on Advanced Packaging*, Vol. 24, No. 3, 334–346, 2001.
6. Ye, X., M. Y. Koledintseva, M. Li, and J. L. Drewniak, "DC power-bus design using FDTD modeling with dispersive media and surface mount technology components," *IEEE Trans. Electromagn. Compat.*, Vol. 43, No. 4, 579–587, Nov. 2001.
7. Ege Engin, A., K. Bharath, and M. Swaminathan, "Multilayered finite-difference method (MFDM) for modeling of package and printed circuit board planes," *IEEE Trans. Electromagn. Compat.*, Vol. 49, No. 2, 441–447, May 2007.
8. Arcioni, P., M. Bozzi, M. Bressan, G. Conciauro, and L. Perregrini, "The BI-RME method: An historical overview," *2014 International Conference on Numerical Electromagnetic Modeling and Optimization for RF, Microwave, and Terahertz Applications (NEMO)*, May 14–16, 2014.
9. Tsang, L. and D. Miller, "Coupling of vias in electronic packaging and printed circuit board structures with finite ground plane," *IEEE Transactions on Advanced Packaging*, Vol. 26, No. 4, 375–384, Nov. 2003.
10. Zhang, Y.-J. and J. Fan, "A generalized multiple scattering method for dense vias with axially-anisotropic modes in an arbitrarily-shaped plate pair," *IEEE Trans. on Microw. Theory and Tech.*, Vol. 60, No. 7, 2035–2045, Jul. 2012.
11. Chang, X. and L. Tsang, "Fast and broadband modeling method for multiple vias with irregular antipad in arbitrarily shaped power/ground planes in 3-D IC and packaging based on generalized Foldy-Lax equations," *IEEE Trans. Compon. Packag. Manuf. Technol.*, Vol. 4, No. 4, 685–696, Apr. 2014.
12. Tsang, L. and S. Huang, "Full wave modeling and simulations of the waveguide behavior of printed circuit boards using a broadband Green's function technique," Provisional U.S. Patent No. 62/152.702, Apr. 24, 2015.
13. Huang, S., "Broadband Green's function and applications to fast electromagnetic analysis of high-speed interconnects," Ph.D. dissertation, Dept. Elect. Eng., Univ. Washington, Seattle, WA, Jun. 2015.
14. Huang, S. and L. Tsang, "Broadband Green's function and applications to fast electromagnetic modeling of high speed interconnects," *IEEE International Symposium on Antennas and Propagation*, Vancouver, BC, Canada, Jul. 2015.
15. Ishimaru, A., *Electromagnetic Wave Propagation, Radiation, and Scattering*, Prentice-Hall, 1991.
16. Tsang, L., J. A. Kong, K. H. Ding, and C. Ao, *Scattering of Electromagnetic Waves, Volume 2, Numerical Simulations*, Wiley, New York, NY, USA, 2001.
17. Tsang, L., H. Chen, C. C. Huang, and V. Jandhyala, "Modeling of multiple scattering among vias in planar waveguides using Foldy-Lax equations," *Microw. Opt. Tech. Lett.*, Vol. 31, 201–208, Nov. 2001.
18. Chen, H., Q. Li, L. Tsang, C. C. Huang, and V. Jandhyala, "Analysis of large number of vias and differential signaling in multi-layered structures," *IEEE Trans. on Microw. Theory and Tech.*, Vol. 51, 818–829, Mar. 2003.
19. Gu, X., B. Wu, C. Baks, and L. Tsang, "Fast full wave analysis of PCB via arrays with model-to-hardware correlation," *IEEE 18th Conference on Electrical Performance of Electronic Packaging and Systems (EPEPS'09)*, 175–178, 2009.
20. Wu, B. and L. Tsang, "Modeling multiple vias with arbitrary shape of antipads and pads in high speed interconnect circuits," *IEEE Microwave and Wireless Comp. Lett.*, Vol. 19, 12–14, 2009.
21. Tsang, L. and X. Chang, "Modeling of vias sharing the same antipad in planar waveguide with boundary integral equation and group T matrix method," *IEEE Trans. Compon. Packag. Manuf. Technol.*, Vol. 3, No. 2, 315–327, Feb. 2013.